THE LONG-TERM PERFORMANCE OF MODEL AUSTENITIC ALLOYS IN HUMID AIR

B. A. Pint
Metals and Ceramics Division
Oak Ridge National Laboratory
Oak Ridge, TN 37831-6156

ABSTRACT

Model austenitic alloys are being studied as part of an alloy development program for high temperature (≥650°C) recuperators for small gas turbine engines. In many cases, the recuperator design requires an alloy foil with both high temperature strength and corrosion resistance in an exhaust gas environment. Previous work showed that type 347 stainless steel would not have sufficient corrosion resistance for this application. Long-term testing is being conducted to better understand the effect of composition on corrosion resistance in humid air at 650°-800°C. Current results show that Fe-20Cr-20Ni with additions of Mn and Si has excellent corrosion resistance in humid air for more than 5,000h at 650° and 700°C. Increasing the Ni content of the alloy is critical to improving corrosion resistance.

Keywords: Stainless steel, gas turbines, recuperators, water vapor, alloy composition

INTRODUCTION

The August 2003 blackout in the United States has bolstered the case for distributed generation as a solution for overloaded transmission lines and improved reliability. One element in the distributed generation portfolio are small (30-250 kW) single-shaft, gas turbine engines or microturbines.[1-2] With a footprint of approximately 3 m x 4 m, these engines could be sited at the user's facility and provide base or peak load electricity while delivering waste heat for climate control or heating water. One potential market uses methane from landfills and sewage plants as fuel.[3]

Microturbines are environmentally attractive because of their low NO_x emissions. However, one of the drawbacks of current microturbines is their relatively low electrical generation efficiency (≈30%) compared to large gas turbines. (An overall efficiency increase is obtained by using the waste heat for other uses.) Thus, one goal of the Department of Energy's Distributed Energy Resources program is to improve the efficiency of next-generation microturbines.[4] Increasing the turbine inlet temperature is a

primary method for increasing engine efficiency. Higher operating temperatures require the selection or development of cost-competitive materials for advanced microturbines.

One of the most critical areas is the recuperator or heat exchanger, which significantly boosts the efficiency of small turbine engines.[5] Increasing the temperature of the recuperator while maintaining durability requirements has proven to be a critical problem. Most recuperator designs have used type 347 stainless steel because of its combination of creep and corrosion resistance. However, it has been well documented that increasing the exposure temperature to ≥650°C has resulted in accelerated attack of type 347 stainless steel due to the presence of water vapor in the exhaust gas.[6-10] Accelerated attack due to water vapor has been observed for both ferritic and austenitic alloys in the 600°-900°C range[11-16] and is currently being investigated by a number of research groups. An increase in the corrosion rate is a particular concern for recuperators because most designs employ thin-walled alloy components having a limited Cr reservoir. The Cr reservoir is an important factor in determining corrosion lifetime because, as Cr is depleted from the foil, at some critical Cr content the foil will no longer be able to form a protective Cr-rich surface oxide. In order to meet recuperator durability goals of ≈40,000 h, a stainless steel must be identified with a low Cr consumption rate and which will make it resistant to accelerated attack.

As described in previous papers,[9,10] the goal of this program is to develop a low-cost alternative to type 347 stainless steel by (1) identifying the base Cr and Ni contents needed for resistance in these environments; (2) identifying beneficial minor alloying additions and (3) combining these results to develop an alloy with sufficient creep and corrosion resistance for the various recuperator designs. The current results on the oxidation performance of model alloys use findings[9,10,17] from the first two stages of the program and are a part of the progress towards meeting the final phase of the program.

EXPERIMENTAL PROCEDURE

Model alloys were vacuum induction melted at Oak Ridge National Laboratory (ORNL) and hot and cold rolled to 1.25 mm sheet. After the final cold rolling step, the sheets were annealed in Ar for 2 min at 1000°C. The annealing conditions were selected to give a uniform grain size similar to that found in commercial stainless steel foils. The grain size was larger than that found in current commercial stainless steel foils (≈10 µm, Figure 1a) but is similar to higher creep strength materials being developed (≈20 µm).[18,19] An example microstructure of one of the model alloys is shown in Figure 1b. The chemical compositions of several model alloys are listed in Table I in order to indicate typical concentrations relative to the nominal values and impurity levels. Oxidation coupons were typically 12 mm x 17 mm and were polished to a 600 grit finish. Prior to oxidation, the specimens were cleaned in acetone and methanol and mass changes were measured using a Mettler-Toledo model AG245 balance after each 100 h cycle at 650°, 700° or 800°C.

Oxidation exposures were conducted in laboratory air and humid (10 vol.% H_2O) air by flowing the gas at 450 cc/min through an alumina tube that was inside a resistively-heated horizontal tube furnace. Distilled water was atomized into the flowing gas stream above its condensation temperature and heated to the reaction temperature within the alumina tube.[6,9] Up to 40 specimens were positioned in alumina boats in the furnace hot zone so as to expose the specimen faces parallel to the flowing gas. After oxidation, selected specimens were Cu-plated and sectioned for metallographic analysis.

RESULTS

The effect of water vapor on a particular alloy is affected by a number of variables including test

temperature, water content and gas velocity.[6,8,14,15] For this work, the gas composition and velocity were held constant and temperature was the primary variable. For the conditions selected, the effect of temperature on Fe-20Cr-20Ni is shown in Figure 2. In humid air, accelerated attack (AA) was observed at 650°C with a large mass gain after 1000 h and at 800°C with an immediate large mass loss due to spallation of the thick reaction product. In dry air, no AA was observed after 500 h at 800°C. Figure 3a shows the thick reaction product formed after 1000 h at 650°C corresponding to a mass gain of over 2 mg/cm^2. However, at 700°C, no AA was observed until after 1500 h of exposure. The measurable effect of the 10% water vapor addition was much less at 700°C than at the higher and lower temperatures. At both 650° and 700°C, an incubation period was observed where no AA occurred. This delay in the onset of AA has been observed in other studies[6,8,10,20] and is also a function of the gas composition and velocity.[15] Depending on the experimental conditions, various studies can report different times to AA or no AA if exposure times are not sufficiently long. Thus, one of the reasons for running long-term tests was to ensure that a material is truly resistant to AA rather than just having an extended incubation period.

Results at 650°C

Previous work on model ferritic alloys showed that Mn and Si were two of the most beneficial minor alloy additions for preventing AA.[9,10] Therefore, a series of model alloys was made with Mn and Si additions. Figure 4 shows the performance of several of these alloys at 650°C in humid air compared to the base model alloy without Mn and Si additions. In each case, the addition of Mn and Si improved the resistance to AA compared to the base alloy. However, with Fe-16Cr-15Ni, the addition of Mn and Si reduced the mass loss compared to the base alloy but did not prevent AA. Figure 3b shows the scale cross-section after 1000 h on Fe-16Cr-15Ni+Mn,Si. Increasing either the Cr or Ni content to 20% and adding Mn and Si prevented the onset of AA to over 5,000 h, Figure 4. Cross-sections of Fe-16Cr-20Ni+Mn,Si and Fe-20Cr-15Ni+Mn,Si after 1,000 h at 650°C are shown in Figures 3c and 3d, respectively. A few large oxide nodules were observed on the former material but, based on the low, long-term mass gain, the nodules did not continue to grow significantly. Only small nodules were observed on Fe-20Cr-15Ni+Mn,Si, Figure 3d. Increasing the Cr and Ni contents to 20% with the additions of Mn and Si resulted in very little mass change after a 5,000 h exposure at 650°C and a uniform thin scale, Figure 3e.

In order to clarify the role of each alloy addition, model alloys were made with various combinations of Mn, Si and La. Figure 5a shows the 650°C performance of a series of alloys with a base combination of Fe-16Cr-15Ni. All of the additions showed less mass loss than the base alloy without additions, but all of the modified alloys showed AA to some degree. Single additions of La or Mn showed the least benefit. Surprisingly, the addition of Si alone showed less mass change than the additions with Si in combination with Mn or Mn and La. In general, these results suggest that the base Fe-16Cr-15Ni alloy is too lean in Cr and Ni to be protective in these conditions. With a base composition of Fe-17Cr-11Ni, a similar inference can be drawn about type 347 stainless steel.

Figure 5b shows the performance of various modifications of a base Fe-20Cr-20Ni alloy at 650°C. Again, single additions of Mn or La did not show a significant beneficial effect. In cross-section, large nodules were observed on Fe-20Cr-20Ni+Mn, Figure 3g. The onset of AA was slowed by the Mn addition but not prevented. Linear mass losses were observed for a Si addition, and a very thin oxide was noted on most of the surface after 1000 h, Figure 3f. The mass losses are attributed to evaporation of Cr from the scale. However, the edges of the specimen showed evidence of the onset of AA. As mentioned above, the addition of Mn and Si showed a low mass change past 5,000 h, indicating a synergistic benefit of having both elements. Adding La in addition to Mn and Si has not shown any additional benefit at

this stage of the testing, Figure 5b.

The first attempt to develop a creep-resistant version of Fe-20Cr-20Ni involved additions of Mn, Si, Nb and several other elements, Table I. The oxidation behavior of this material also is shown in Figure 5b. The mass gain was higher than the model alloy with only Mn and Si additions, but no AA was observed after more than 5,000 h. The higher mass gain is attributed to the higher Mn content, which appears to have resulted in a thicker scale but no signs of AA, Figure 3h.

Results at 700°C

Figure 6 shows the long-term performance for some of the modified model alloys at 700°C. As at 650°C, the additions of Mn and Si significantly improved the performance of the base alloys with either 20Cr or 20Ni. However, the leanest alloy, Fe-16Cr-15Ni, showed AA with high mass losses after 1000 h. The specimen with Fe-16Cr-20Ni+Mn and Si began to show increased mass gain after 4000 h compared to the alloys with 20Cr. After 1000 h, a cross-section of the scale did not show any indication of AA (Figure 7a). Likewise, a thin scale formed on Fe-20Cr-15Ni+Mn,Si after 1000 h (Figure 7b), although an occasion nodule was noted. The low mass change for this alloy after 5,000 h, suggests that these small nodules did not continue to grow. A similar thin scale was observed for Fe-20Cr-20Ni+Mn,Si (Figure 7c). A slightly thinner scale was observed on the specimen of Fe-20Cr-20Ni+Si after 1,000 h, (Figure 7d). Unlike the other alloys with both Mn and Si additions, this alloy has shown a continuous mass loss past 5000 h, but no indication of AA(Figure 6). Finally, the creep-resistant version of Fe-20Cr-20Ni, also has shown no sign of AAafter 5,000 h. As at 650°C, the scale formed on this alloy after 1000 h was much thicker than the alloys with fewer additions (Figure 7e).

Accelerated testing results

Since the 100 h cyclic testing at lower temperatures (650°-700°C) failed to differentiate some of the model alloys after more than 5,000 h of testing, additional tests were conducted at 800°C to accelerate the oxidation process. These exposures again showed the beneficial effect of Mn and Si additions (Figure 8a). At this temperature, each of the modified alloys eventually showed AA. The specimen of Fe-16Cr-15Ni+Mn,Si showed AA after 200 h. A cross-section of the scale after 500 h is shown in Figure 9a. By increasing the Cr and Ni contents to 20%, the time to AA was increased to over 2000 h. (The onset of mass losses for this alloy is clearly seen with the expanded y-axis in Figure 8b.) A cross-section of the scale formed on Fe-20Cr-20Ni+Mn,Si after 3000 h is shown in Figure 9b. Even after 3000 h, the extent of AAwas less on the more highly alloyed material. The specimen of Fe-16Cr-20Ni+Mn,Si began to show AA after 1300 h and the scale after 2,000 h is shown in Figure 9c. The specimen of Fe-20Cr-15Ni+Mn,Si began to show AAafter 1500 h and its scale after 2000 h is shown in Figure 9d. To illustrate the change between protective scale formation and AA, the scale formed on Fe-20Cr-15Ni+Mn,Si after 500 h is shown in Figure 9e. Note the change in magnification as the ≈3 µm thick scale after 500 h increases to >40 µm after 2000 h.

Figure 8b shows the performance of the various versions of Fe-20Cr-20Ni tested at 800°C. As at lower temperatures, the single additions of Mn and La did not provide a substantial benefit and the specimen with only Si added showed a continuous mass loss but no AA after 3,000 h. As noted above, the specimen with Mn and Si began to show mass loss associated with the onset of AA after 2,000 h. Interestingly, the alloy with La as well as Mn and Si did not show AA until 3,000 h. The scale formed on this alloy after 500 h is shown in Figure 9f. The scale is thinner than that formed on Fe-20Cr-15Ni+Mn,Si after 500 h suggesting a beneficial effect of La at this higher temperature. The creep resistant version of Fe-20Cr-20Ni has not shown AA after testing for more than 4,000 h at 800°C. The

thicker scale formed on this alloy (indicated by the higher mass gain) may be beneficial in preventing AA under these conditions.

Since increasing the test temperature to 800°C may be a questionable strategy in accelerating the evaluation process,[9] another possibility is to increase the cycle frequency (i.e. decrease the time of each cycle) of the test at a lower temperature. A higher Figure 10 shows results for these model alloys during 1h cycles at 700°C in humid air. Using 1h cycles has led to the onset of AA in several alloys that did not show similar attack during 100 h cycles (Figure 6). In particular, Fe-16Cr-20Ni+Mn,Si showed AA after ≈300 h and Fe-20Cr-15Ni showed AA after 500 h, first with a mass increase followed by spallation of the thicker scale. Surprisingly, the Fe-20Cr-20Ni+Si specimen also began to show AAin less than 500 h. To confirm this result, a second specimen also was tested and showed similar behavior (Figure 10). As at 800°C, the specimens showing the longest life all were based on Fe-20Cr-20Ni with Mn and Si additions. The creep-resistant version showed no indication of AAafter 3,000, 1h cycles. The specimen of Fe-20Cr-20Mn+Mn,Si,La did not show AAuntil 2,000 cycles. The specimen with only Mn and Si additions began to show some mass gains and losses after 1500 h, but was not as severely attacked as some of the lower alloyed specimens.

DISCUSSION

The current results clearly show the benefits of increasing the Cr and Ni contents as well as additions of Mn and Si. At each of the conditions used, specimens of Fe-16Cr-15Ni+Mn,Si showed the earliest onset of AA. The increased resistance of specimens of Fe-20Cr-15Ni+Mn,Si and Fe-16Cr-20Ni+Mn,Si demonstrate that higher levels of either Cr or Ni are needed. However, in terms of developing a replacement for type 347 stainless steel which will meet the durability goals of the Advanced Microturbine program, the Fe-20Cr-20Ni specimen appears to be the best candidate. Of course, even higher Cr and Ni would provide more resistance to this environment but higher alloyed materials will be more expensive and higher Cr contents can lead to problems with decreased strength (i.e. type 310 stainless) and embrittlement due to σ phase formation.[18] Should Fe-20Cr-20Ni not have sufficient durability in foil form, the next step would be an alloy based on Fe-20Cr-25Ni.

The reason for the beneficial effect of Ni in the scale has not been determined. Several hypotheses can be proposed, including reduction of the Cr depletion profile in the alloy or decreasing the solubility of O in the metal.[17] Previous work on Fe-20Cr-25Nb showed that depletion of Cr at the metal-scale interface to ≈14% led to increased rates of attack.[21] Initial attempts to compare Cr depletion profiles in model alloys with various Ni contents has not shown any significant difference after exposure of Fe-20Cr-10Ni and Fe-20Cr-30Ni at 650°C for 100 h. This issue will require additional experiments designed to address various hypotheses.

The improvements with the addition of Si are attributed to the formation of a SiO_2 inner layer.[16,22,23] The formation of such a layer could slow the reaction rate thereby reducing the depletion of Cr in the alloy. However, it also is possible that Si changes diffusivities in the alloy leading to its beneficial effect. The addition of Mn has been reported to reduce Cr evaporation due to the formation of a Mn rich outer layer.[24] When added individually, Si appeared more effective in improving resistance to AA than Mn alone. However, the combination of Mn and Si appeared to produce the best results in these tests. One possible problem for Si alone at 650°C is that slowing the scale growth at this temperature simply results in less scale to evaporate, leading to early onset of AA. Adding Mn with Si results in a thicker scale due to the formation of Mn-rich spinel-type oxides which may be more resistant to evaporative losses. Additions of La alone had very little effect at any of the temperatures tested.

However, the addition of La with Mn and Si did show an improvement in the accelerated testing (Figures 8b and 10). The improvement with the addition of La at 800°C could be attributed to a reactive element effect,[25-27] such as the thinner scale observed (Figure 9f). If La alone simply reduced the scale growth rate, this might be ineffective due to the problem of scale evaporation. However, in combination with a Mn-rich outer layer and a SiO_2 inner layer, a thinner Cr-rich scale may have a beneficial effect. The La effect is less likely to be operative at lower temperatures like 650°C where typical reactive element mechanisms are not operable.[26] The creep resistant version of Fe-20Cr-20Ni showed higher mass gains than the model alloys but no indication of a problem with AA. One issue with this composition is that the thicker scale may not be a problem with the 1-1.25 mm thick sheet specimens used in this study, although a higher Cr consumption rate could be problematic for foil specimens with a more limited reservoir of Cr.

One problem with the current results is that correlation with the performance of foil materials is not straight forward. Trying to draw conclusions from mass gains and scale thickness could lead to incorrect conclusions due to the additional complication of scale evaporation. That is one reason why no rate constants were calculated from these data. The best way to predict lifetime may be to determine the Cr consumption rate from a foil as a function of exposure conditions. Changes in the Cr consumption rate determined in this way would incorporate all effects and would give a better measure of the effectiveness of the minor alloy additions. For instance, adding more Mn may increase the mass gain due to the formation of more evaporation-resistant, Mn-rich oxide, but this may not have a beneficial effect on lifetime if it increases the overall Cr consumption rate. As this program progresses, it also will be desirable to move towards a more relevant test environment. Prior to engine testing, an additional evaluation step will be the microturbine test facility at ORNL[28] which can expose foil specimens to the exhaust gas from a microturbine under controlled temperature and pressure to evaluate performance.

SUMMARY

Long-term testing of model austenitic alloys in air + 10%H_2O at 650°- 800°C is assisting in the development of more corrosion-resistant stainless steels to replace type 347 stainless steel the recuperator of advanced microturbines. Higher Cr or Ni contents increase the resistance to this environment. Model alloys with various combinations of minor additions showed that a combination of Mn and Si produces the best resistance to this environment. The current focus of development is alloys based on Fe-20Cr-20Ni+Mn,Si which show excellent resistance to this environment at 650°-700°C. This alloy appears to have the best chance of meeting the durability and cost targets of the program. Future work will focus on the effect on corrosion resistance of minor alloy additions needed to improve the creep strength of this alloy and testing of foil specimens of this composition.

ACKNOWLEDGMENTS

The authors wish to thank J. D. Vought at ORNL for casting the alloys, G. W. Garner for performing the oxidation exposures, H. Longmire for performing the metallography and L. Walker for performing the microprobe work. P. F. Tortorelli and I. G. Wright at ORNL reviewed the manuscript. The research was sponsored by the U.S. Department of Energy, Office of Distributed Energy Resources under contract DE-AC05-00OR22725 with UT-Battelle, LLC.

REFERENCES

1. J. H. Watts, Global Gas Turbine News 39(1), (1999): pp.4-8.
2. S. L. Hamilton, Modern Power Systems 19(9), (1999): pp.21-22.

3. Industry News, Pollut. Eng. 33(8), (2001): p.7.
4. Advanced Microturbine Systems Program, Plan for Fiscal Years 2000 Through 2006, U. S. Department of Energy, Office of Energy Efficiency and Renewable Energy, Office of Power Technologies, Washington, D. C. (March 2000).
5. C. F. McDonald, Applied Thermal Eng. 23, (2003): pp.1463-87.
6. B. A. Pint and J. M. Rakowski, NACE Paper 00-259, Houston, TX, presented at NACE Corrosion 2000, Orlando, FL, March 2000.
7. J. M. Rakowski and B. A. Pint, NACE Paper 00-517, Houston, TX, presented at NACE Corrosion 2000, Orlando, FL, March 2000.
8. J. M. Rakowski, ASME Paper 2001-GT-360, presented at the International Gas Turbine & Aeroengine Congress & Exhibition, New Orleans, LA, June 4-7, 2001.
9. B. A. Pint, R. Peraldi and P. F. Tortorelli, NACE Paper 03-499, Houston, TX, presented at NACE Corrosion 2003, San Diego, CA, March 2003.
10. B. A. Pint and R. Peraldi, ASME Paper #GT2003-38692, presented at the International Gas Turbine & Aeroengine Congress & Exhibition, Atlanta, GA, June 2-5, 2003.
11. D. Caplan and M. Cohen, Corrosion 15, (1959): pp.57-62.
12. C. T. Fujii and R. A. Meussner, J. Electrochem. Soc. 110, (1963): p.1195; 111, (1964): p.1215.
13. D. L. Douglass, P. Kofstad, A. Rahmel and G. C. Wood, Oxid. Met. 45, (1996): pp.529-45.
14. H. Nickel, Y. Wouters, M. Thiele and W. J. Quadakkers, Fresenius J. Anal. Chem. 361, (1998): pp.540-4.
15. H. Asteman, J.-E. Svensson, M. Norell and L.-G. Johansson, Oxid. Met. 54, (2000): p.11-26.
16. S. Henry, A. Galerie and L. Antoni, Mater. Sci. Forum 369-372, (2001): p.353-60.
17. R. Peraldi and B. A. Pint, submitted to Oxid. Met. (2003).
18. P. J. Maziasz, R. W. Swindeman, J. P. Montague, M. Fitzpatrick, P. F. Browning, J. F. Grubb and R. C. Klug, Mater. High Temp. 16, (1999): p.207-12.
19. P. J. Maziasz and R. W. Swindeman, J. Eng. Gas Turbines and Power 125, (2003): p.51.
20. J. Shen, L. Zhou and T. Li, Oxid. Met. 48, (1997): p.347-56.
21. H. E. Evans and R. C. Lobb, Corrosion Science 24, (1984): pp.223-36.
22. K. Tamura, T. Sato, Y. Fukuda, K. Mitsuhata, H. Yamanouchi, Heat Resistant Materials II, K. Natesan, P. Ganesan and G. Lai eds., ASM International, Materials Park, OH, 1995, p.33-9.
23. B. A. Pint, K. L. More and P. F. Tortorelli, ASME Paper 2002-GT-30543, presented at the International Gas Turbine & Aeroengine Congress & Exhibition, Amsterdam, Netherlands, June 3-6, 2002.
24. W. J. Quadakkers, T. Malkow, J. Piron-Abellan, U. Flesch, V. Shemet and L. Singheiser, Proc. 4th Eur. Solid Oxide Fuel Cell Forum, Vol. 2, A. J. McEvoy ed. (Elsevier, Amsterdam, 2000) p.827-36.
25. A. Strawbridge and P. Y. Hou, Materials at High Temperature 12, (1994): pp.177-81.
26. B. A. Pint, Oxidation of Metals 45, (1996): pp.1-37.
27. J. Quadakkers and L. Singheiser, Mater. Sci. Forum 369-72, (2001): pp.77-92.
28. E. Lara-Curzio, P. J. Maziasz, B. A. Pint, M. Stewart, D. Hamrin, N. Lipovich and D. DeMore, ASME Paper #2002-GT-30581, presented at the International Gas Turbine & Aeroengine Congress & Exhibition, Amsterdam, Netherlands, June 3-6, 2002.

TABLE 1
ALLOY CHEMICAL COMPOSITIONS (WEIGHT %) AND AVERAGE GRAIN SIZES (µm)

Material	Cr	Ni	Mn	Si	C	N	Nb	Ti	Mo	Other	average grain size
Type 347	17	11	1.6	0.6	0.04	0.02	0.6	0.04	0.1		5 µm
Fe-20Cr-20Ni	19.7	20.1	<	0.01	<	<	<	<	<		14
Fe-16Cr-15Ni	15.8	14.8	<	<	0.002	<	<	<	<		24
Fe-16Cr-15Ni+MS	15.8	14.8	1.76	0.24	<	<	<	<	<		21
Fe-16Cr-20Ni+MS	15.8	19.7	1.72	0.24	0.003	0.001	<	<	<		26
Fe-20Cr-15Ni+MS	19.8	14.9	1.70	0.24	0.001	0.007	<	<	<		20
Fe-20Cr-20Ni+MS	19.8	19.8	1.69	0.25	<	0.003	<	<	<		25
Fe-20Cr-20Ni+Mn	20.0	19.8	1.47	0.01	0.002	0.001	<	<	0.01		17
Fe-20Cr-20Ni+Si	19.9	19.7	<	0.23	0.001	0.005	<	<	<		30
Fe-20Cr-20Ni+La	20.3	19.7	<	<	0.001	0.001	<	<	<	0.10 La	12
Fe-20Cr-20Ni+MSL	20.2	19.9	1.61	0.22	0.001	0.011	<	<	<	0.12 La	14
Fe-20Cr-20Ni+etc.	20.9	20.8	3.8	0.24	0.08	0.18	0.25	<	0.31	0.3 Cu, 0.3Co	55
Fe-16Cr-15Ni+Mn	16.0	15.0	1.66	0.01	0.002	0.001	<	<	<		21
Fe-16Cr-15Ni+Si	16.2	14.7	<	0.17	<	0.001	<	<	<		25
Fe-16Cr-15Ni+La	16.1	14.9	<	0.01	0.001	0.02	<	<	<	0.17 La	21
Fe-16Cr-15Ni+MSL	17.0	14.1	1.74	0.24	0.002	0.001	<	<	<	0.17 La	27

< indicates below the detectability limit of <0.01% or <0.001% for interstitials

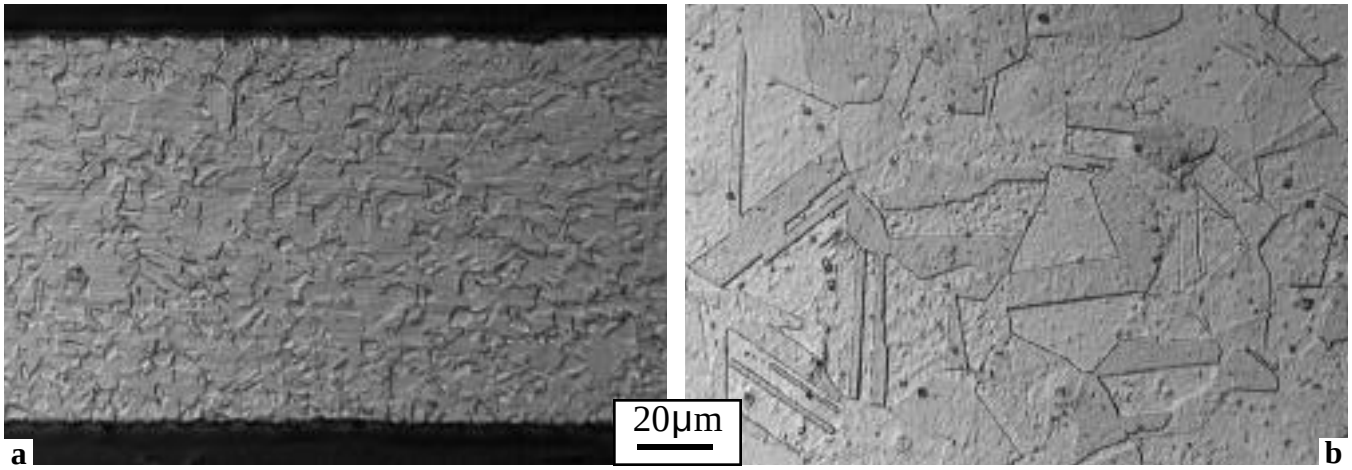

FIGURE 1. Light microscopy of (a) commercial type 347 stainless steel and (b) model Fe-20Cr-20Ni+Mn,Si.

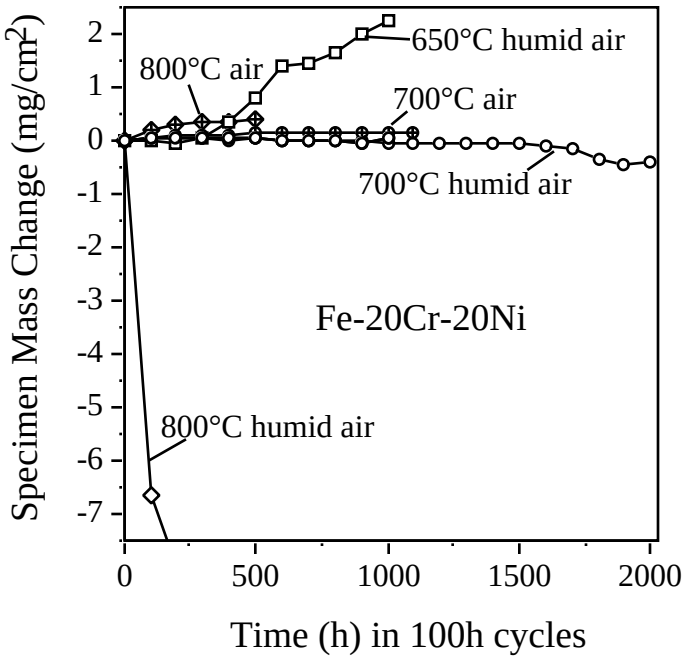

FIGURE 2. Mass change of Fe-20Cr-20Ni specimens during 100 h cycles at 650°, 700° and 800°C in dry air or air plus 10% water vapor. The accelerated attack with the addition of water vapor was more significant at 650° and 800°C than at 700°C. Lower mass gains were noted in dry air.

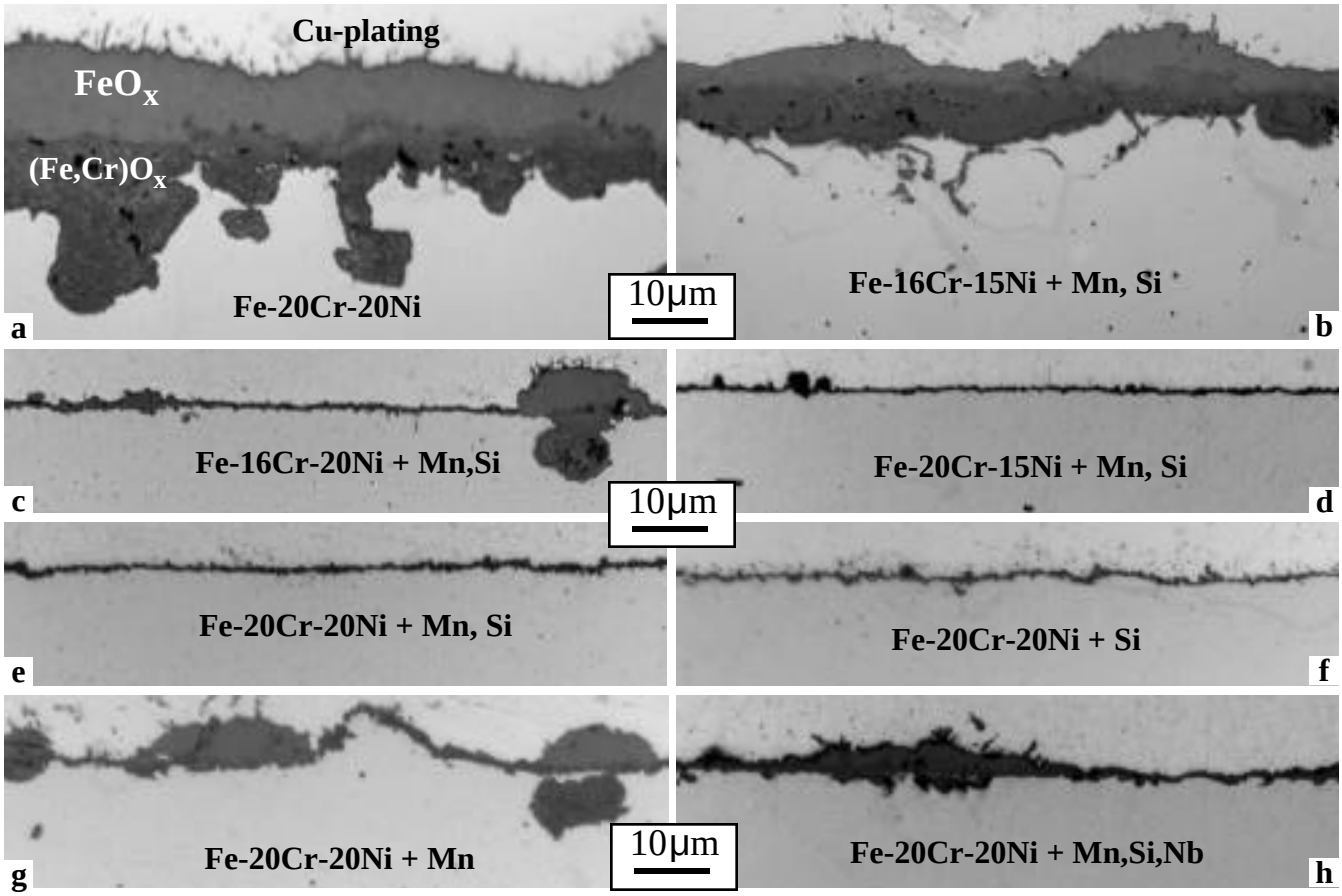

FIGURE 3. Light microscopy of polished cross-sections of model alloys oxidized for 1000 h at 650°C in humid air (a) Fe-20Cr-20Ni, (b) Fe-16Cr-15Ni+Mn,Si, (c) Fe-16Cr-20Ni+Mn,Si, (d) Fe-20Cr-15Ni+Mn,Si, (e) Fe-20Cr-20Ni+Mn,Si, (f) Fe-20Cr-20Ni+Si, (g) Fe-20Cr-20Ni+Mn, and (h) Fe-20Cr-20Ni+Mn,Si,etc.

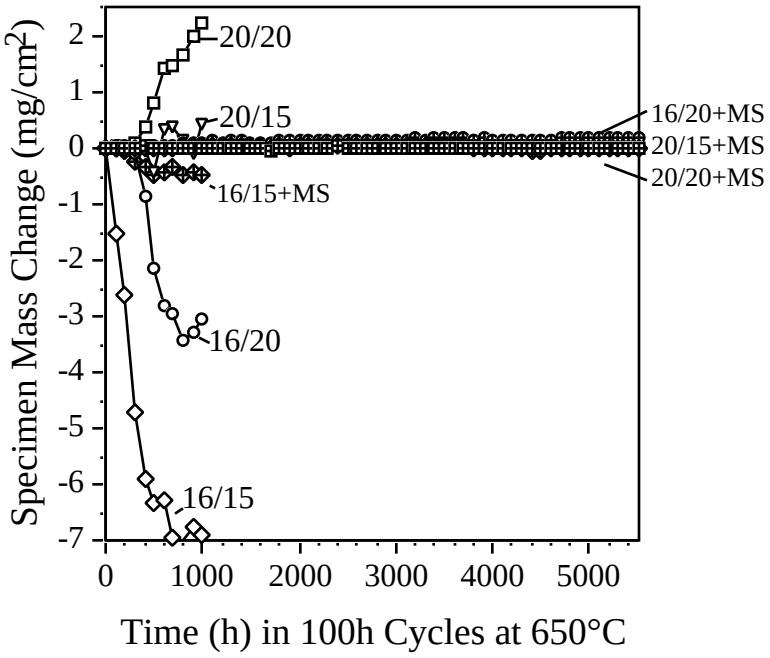

FIGURE 4. Specimen mass changes for model Fe-Cr-Ni alloys (specified by their Cr/Ni contents) during 100 h cycles at 650°C in air plus 10%H_2O. Designations with "+MS" indicate Mn and Si additions.

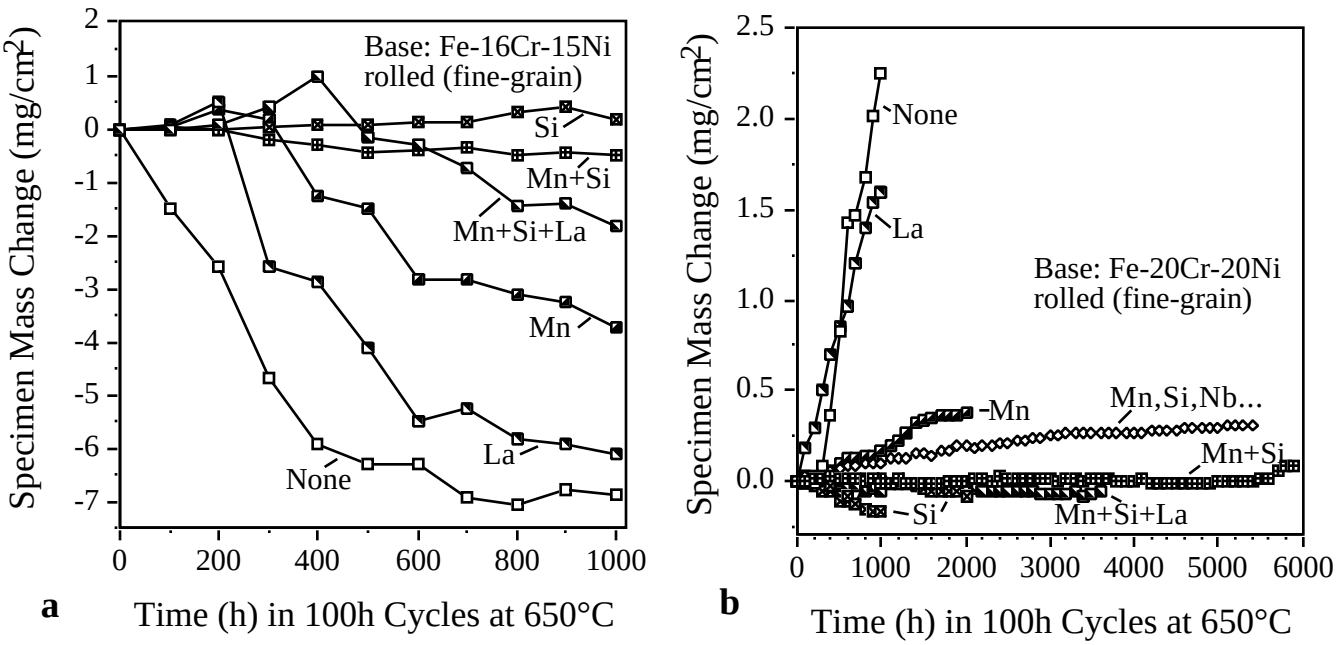

FIGURE 5. Specimen mass changes for model Fe-Cr-Ni alloys during 100 h cycles at 650°C in air plus 10%H_2O, (a) alloys with a base composition of Fe-16Cr-15Ni and (b) alloys with a base composition of Fe-20Cr-20Ni.

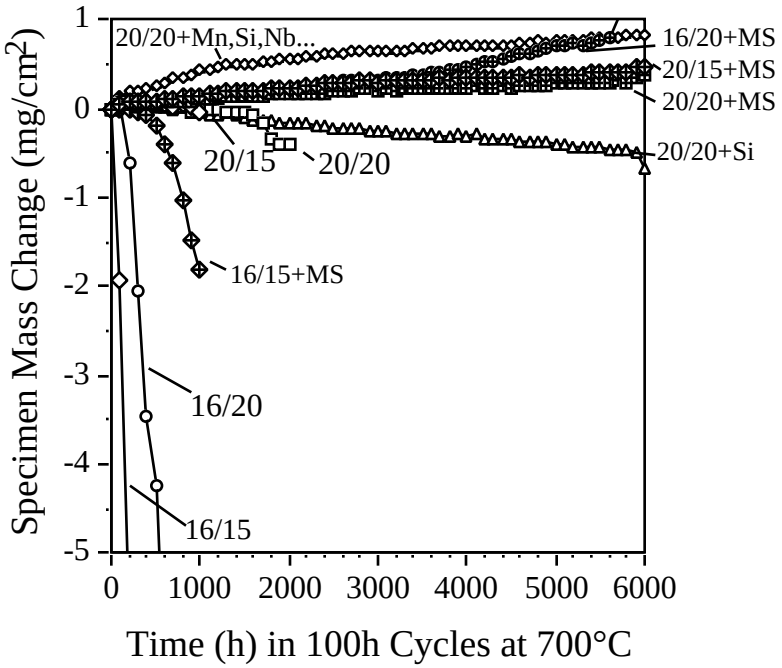

FIGURE 6. Specimen mass changes for model Fe-Cr-Ni alloys (specified by their Cr/Ni contents) during 100 h cycles at 700°C in air plus 10%H_2O. Designations with "+MS" indicate Mn and Si additions.

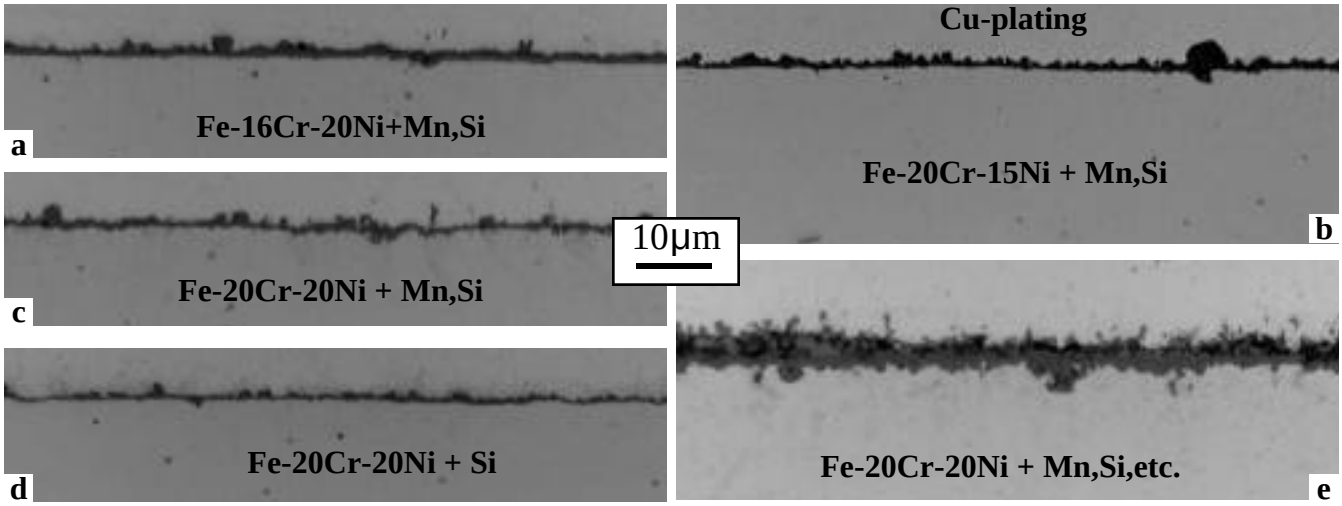

FIGURE 7. Light microscopy of polished cross-sections of model alloys oxidized for 1000 h at 700°C in humid air (a) Fe-16Cr-20Ni+Mn,Si, (b) Fe-20Cr-15Ni+Mn,Si, (c) Fe-20Cr-20Ni+Mn,Si, (d) Fe-20Cr-20Ni+Si, and (e) Fe-20Cr-20Ni+Mn,Si,etc.

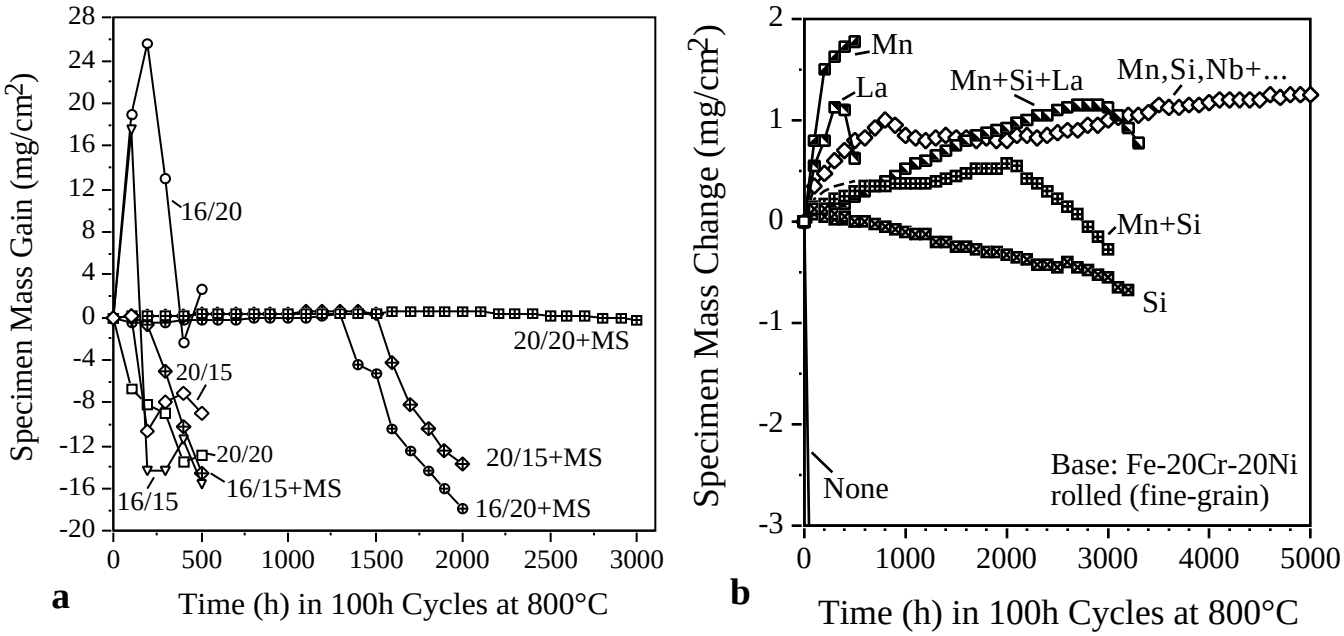

FIGURE 8. Specimen mass changes for model Fe-Cr-Ni alloys during 100 h cycles at 650°C in air plus 10%H_2O, (a) alloys with and without Mn and Si additions and (b) alloys with a base composition of Fe-20Cr-20Ni. Designations with "+MS" indicate Mn and Si additions.

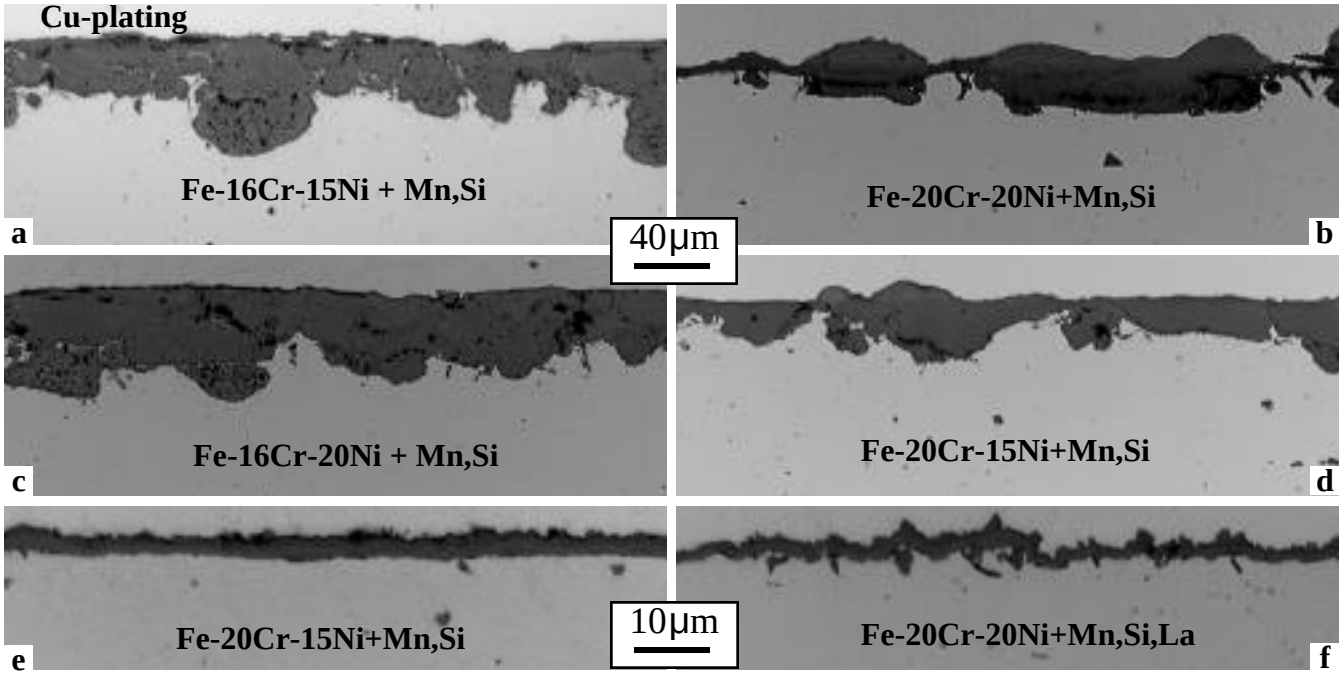

FIGURE 9. Light microscopy of polished cross-sections of model alloys oxidized for at 800°C in humid air (a) Fe-16Cr-15Ni+Mn,Si after 500 h, (b) Fe-20Cr-20Ni+Mn,Si after 3000 h, (c) Fe-16Cr-20Ni+Mn,Si after 2000 h, (d) Fe-20Cr-15Ni+Mn,Si after 2000 h, (e) Fe-20Cr-15Ni+Mn,Si after 500 h and (f) Fe-20Cr-20Ni+Mn,Si,La after 500 h.

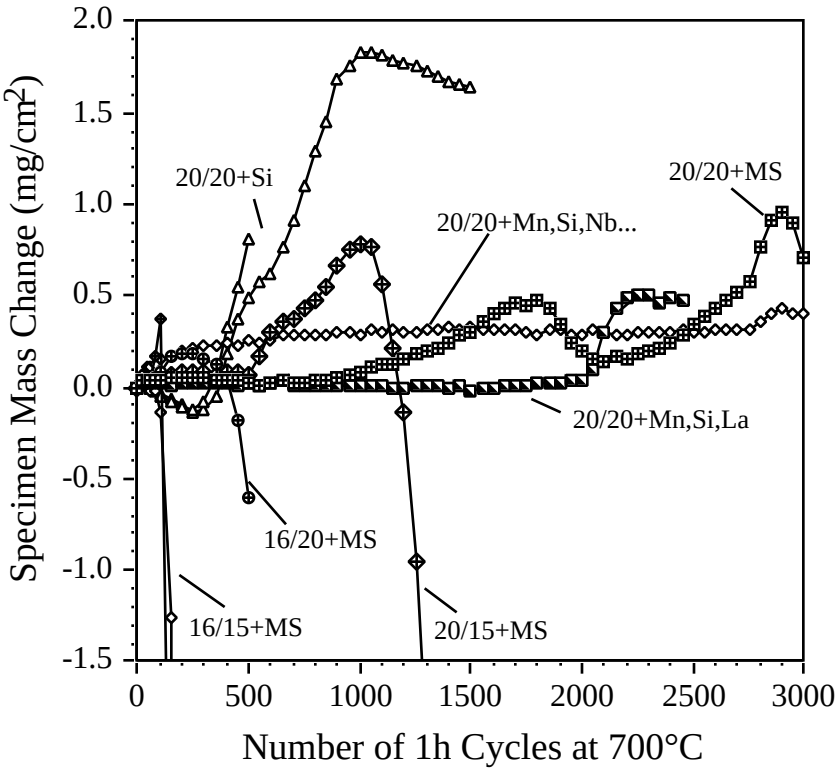

FIGURE 10. Specimen mass changes for model Fe-Cr-Ni alloys (specified by their Cr/Ni contents) during 1h cycles at 700°C in air plus 10%H_2O. Designations with "+MS" indicate Mn and Si additions.